

Ab initio molecular-dynamics simulations of electronic structures and characteristics of Cu/SiO₂/Pt memristive stack

Y. X. Peng^{a,*}, L. Wang^b

^a*School of Information Engineering, Nanchang Hangkong University, 330063, Nanchang, P. R. China*

^b*School of Electrical and Optical Engineering & School of Microelectronics, Nanjing University of Posts and Telecommunications, 210003, Nanjing, P. R. China*

Memristor, as the fourth passive fundamental circuitry element, has recently received considerable attention due to its appealing prospect for in-memory computing and neuromorphic computing applications. Numerous memristive materials, such as metal oxides, chalcogenides, amorphous silicon, carbon, and polymer nanoparticle materials, have been under intensive research. Within the memristive families, metal oxides attain more attention due to their great scaling, fast switching speed, low power consumption, and long endurance. However, the memristive mechanism and electronic characteristics of the metal oxides still remain controversial. To address this issue, we here investigated the electronic structure and electronic characteristics of a typical memristive stack (i.e., Cu/SiO₂/Pt) based on newly developed density functional theory and ab initio molecular-dynamics simulations. Calculated results reveal that the energy barriers required to be overcome for Cu ions to diffuse through Cu electrode, SiO₂ active layer, and Pt electrode, are 0.6 eV, 1 eV, and 1.63 eV, respectively. This results in an overall barrier of ~ 1.63 eV for entire Cu/SiO₂/Pt stack. Both ion and electron conductivities of the Cu/SiO₂/Pt stack are found temperature dependent, while the electron conductivities arising from calculated density of states and band structures, is much higher than the ion conductivity. This obviously facilitates the diffusion of Cu ions and thus can explain the memristive behaviour of the studied device.

(Received November 9, 2021; Accepted February 7, 2022)

Keywords: Cu, SiO₂, Electrical conductivity, Memristive, Ab initio molecular dynamics

1. Introduction

Digital computer is undoubtedly one of the greatest inventions during human's history. Data from external environment can be input by peripheral devices, stored inside memories, and processed by central processing unit (CPU). Static random access memory (SRAM) and dynamic RAM are two most important on-chip memory components of the modern computer, which are usually employed to store the most frequently used data by CPU. It should be noted that SRAM

* Corresponding author: *21026@nchu.edu.cn

<https://doi.org/10.15251/JOR.2022.181.83>

and DRAM are generally made of complementary-metal-oxide-semiconductor (CMOS) components, whose integration density is determined by Moore's law [1, 2]. However, Moore's law is most recently reported to approach its limits [3, 4], which thus severely impairs the computing performances of the digital computer. For this reason, it is timely to explore some innovative storage devices to replace conventional CMOS-based SRAM and DRAM.

Developments of semiconductor manufacture and materials synthesis technologies fortunately lead to some promising candidates as substitutions for SRAM and DRAM. These candidates can be attributed to non-volatile memory category that can be further classified into ferroelectric RAM [5, 6], magnetic RAM [7, 8], phase-change RAM [9, 10], and resistive RAM [11, 12]. These non-volatile RAMs exhibit several advantageous features when compared to CMOS-based RAMs, including superb scaling [13], ultra-fast switching speed [14], ultra-small energy consumption [15], and long endurance [16]. Within the non-volatile memory family, resistive RAM has recently gained more popularity than its compatriots, particularly owing to its suitability for memristor applications. Memristor has been widely considered as the fourth passive fundamental circuitry element in addition to resistor, inductor, and capacitor [17]. The most appealing trait of memristor arises from its ability to simultaneously process and store data at the same location. As this trait attractively coincides with that of the biological brain, it is natural to conceive that memristor can be used to imitate the biological neurons and synapses. The prosperity of memristor technology stems from the pioneering achievement of the TiO_2 memristor that is considered as one typical resistive metal oxide [18]. Considerable research efforts are therefore devoted to exploring memristor devices using various resistive materials, mainly focused on TiO_2 [19, 20], HfO_2 [21, 22], ZrO_2 [23, 24], TaO_2 [25, 26], and SiO_2 [27, 28]. More importantly, aforementioned storage characteristics of the resistive RAM using metal oxides closely match the biological response of the human brain, further proving their potential for in-memory computing and neuromorphic computing applications.

Although a variety of resistive RAMs based on metal oxides show the exciting memristive behaviour, the physical mechanism that governs such behaviour still remains vague and controversial. One of the most plausible interpretations ascribes the memristive mechanism of the resistive RAMs to the so-called electric pulse induced resistive switching effect (EPIR) [29]. According to the EPIR hypothesis, a positive electric bias enables the formation of a conductive filaments (CFs) consisting of Cu ions. Such filament connects the top active electrode with the bottom inert electrode, which results in the low resistance state. The negative bias however ruptures the previously formed filament and switches the device back to the high resistance state. The EPIR hypothesis provides an understandable explanation to the resistive switching and memristive behaviours of the resistive RAM, whereas it lacks the correlated experimental evidence. This can be attributed to the tiny size of the CFs that are hardly observed even by the transmission electron microscopy. To address this issue, we adopt density functional theory (DFT) and *ab initio* molecular simulations (AIMD) here to investigate the electronic structure (i.e., density of state, energy band, and energy barrier), and electronic properties (i.e., ion conductivity and electrical conductivity) of one typical resistive RAM stack, namely copper (Cu)/silicon dioxide (SiO_2)/platinum (Pt) during the diffusion of Cu ions through the entire stack. Results from our simulations cannot only accurately unravel the cause of the CFs formation, but also help researchers to deeply comprehend the physical mechanism behind the memristive behaviour of the resistive RAM using metal oxides.

2. Methods

To perform simulations, we use density functional theory (DFT) method and corresponding well-applied Vienna Ab initio Simulation Package (VASP) software to perform structural optimization calculations [30]. We adopt the cutoff energy of 400 eV, and Perdew-Burke-Ernzerhof (PBE) functional with the generalized gradient approximation (GGA) was used to describe the electronic properties [31, 32]. We also use the projector augmented wave (PAW) to describe the core-electron interactions. The force threshold is set to be 0.05 eV Å⁻¹, and the energy threshold is chosen to be 10⁻⁴ eV. The k-points are defined as 1×1×1 following Monkhorst-Pack scheme. We first optimize the lattice parameters of Pt, SiO₂ and Cu, and subsequently perform the construction of three layered surfaces. To build the Cu/SiO₂/Pt heterojunction, we first build three-layer structure of the Pt (100) and Cu (100) surfaces, which are respectively located at the bottommost and topmost layer of the junction. A seven-layer SiO₂(100) structure is built subsequently and is deposited at the middle layer of the junction. The AIMD approach is employed to probe the energy change during Cu ion diffusion process. The general settings of the AIMD are considered the same as those in DFT calculations. The time step of the AIMD is set to be 1 fs, and the heterojunction structure first undergo relaxation at 300 K to equilibrate its structures with NVT ensemble for at least 5 ps.

After relaxation, a Cu atom is placed at the Cu (100) interfacial side of the defined heterojunction. This excessive Cu atom is used to simulate the energy change of the ion diffusion. We take advantage of a slow-growth method to describe the energy change during the diffusion process. In this method, we set a collective variable (CV) ξ , which is the average length between four topmost Pt atoms and the Cu atom diffusing. Four Pt atoms are arbitrarily selected, and we chose four Pt atoms, which show the furthest distance from the Cu atom. This ensures that the ξ has a large value at the initial state, thus essential to keep the Cu atom diffusing smoothly. When the diffusion process begins, ξ tends to be smaller, and the free-energy difference between states a and b can be computed by integrating the free-energy gradients over a connecting path:

$$\Delta A_{a \rightarrow b} = \int_{\xi(a)}^{\xi(b)} \frac{\partial A}{\partial \xi} d\xi \quad (1)$$

where A is the free energy at a given state of CV.

To calculate the change of A as a function of ξ , we have:

$$\left(\frac{\partial A}{\partial \xi_k} \right)_{\xi^*} = \frac{1}{\left(|\mathbf{Z}|^{-\frac{1}{2}} \right)_{\xi^*}} \left\langle |\mathbf{Z}|^{-\frac{1}{2}} \left[\lambda_k + \frac{k_B T}{2|\mathbf{Z}|} \sum_{j=1}^r (\mathbf{Z}^{-1})_{k_j} \sum_{i=1}^{3N} m_i^{-1} \nabla_i \xi_j \cdot \nabla_i |\mathbf{Z}| \right] \right\rangle_{\xi^*} \quad (2)$$

where Z indicates the tensor of the system mass.

According to above approach, the Cu atom diffusion begins and ends at the Cu (100) side and the Pt (100) side, respectively, and the forces at each step can be integrated along the change of ξ , which is the overall energy change of the diffusion process. In our work, the increment of changing the ξ is 0.001 Å/step. The Cu/SiO₂/Pt heterojunction structure is shown as in Figure 1, and the simulation environment is set at 300 K.

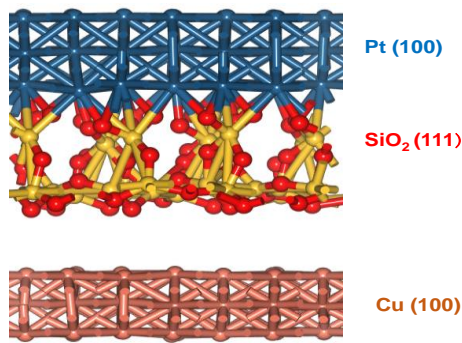


Fig. 1. Relaxed structure of Cu/SiO₂/Pt heterojunction.

3. Results and discussions

The energy change of the Cu atom diffusion across the Cu/SiO₂/Pt heterojunction is first calculated with respect to different transitional states. To simulate the ion diffusion process of Cu, we place a Cu atom at the Cu (100) side of the heterojunction, and implement a so-called slow growth method combined with aforementioned defined CV to make the diffusion take place. The energy change of the diffusion across the Cu layer is plotted against the CV, as shown in Figure 2(a), and resulting transitional states are schematically interpreted in Figure 2(b). It is witnessed that the adsorption of the Cu ion at the Cu (100) surface (from IS to IM-1) has an energy release of ~ -0.3 eV, followed by the embedment of the Cu ion into the first layer of the Cu (100) surface (from IM-1 to IM-2) with a barrier of 0.7 eV. At the IM-3 state, the diffusing Cu ion reaches the interior region of Cu (100) structure. As the Cu ion diffuses toward Pt (100) side, the system energy increases, and the overall energy increase from IS to FS is ~ 1.7 eV. Considering that the diffused Cu ion crosses three-layer Cu (100), it is expected that the diffusing energy change may be ~ 0.6 eV per Cu (100) layer. This result is also consistent with the energy change from IM-1 to IM-2.

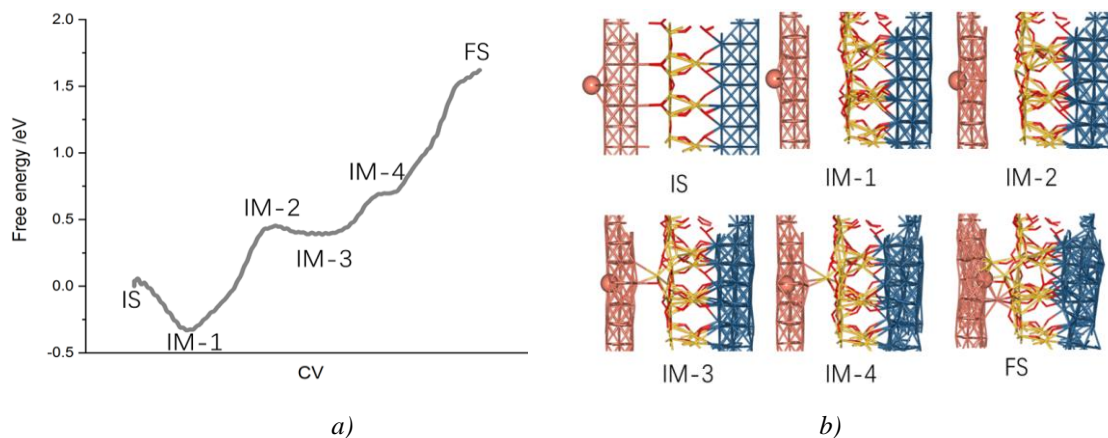


Fig. 2. (a) The energy changes as a function of CV during diffusion from vacuum region to the interface of Cu (100)/SiO₂ (111), and (b) the structure snapshots of different transitional states where the energy changes are calculated. IS, IM, and FS correspond to initial state, intermediate and transition state, respectively. For IM, we chose four representatives states. The diffusing Cu ion is denoted as the ball and stick model, while the heterojunction structure is shown as the stick model.

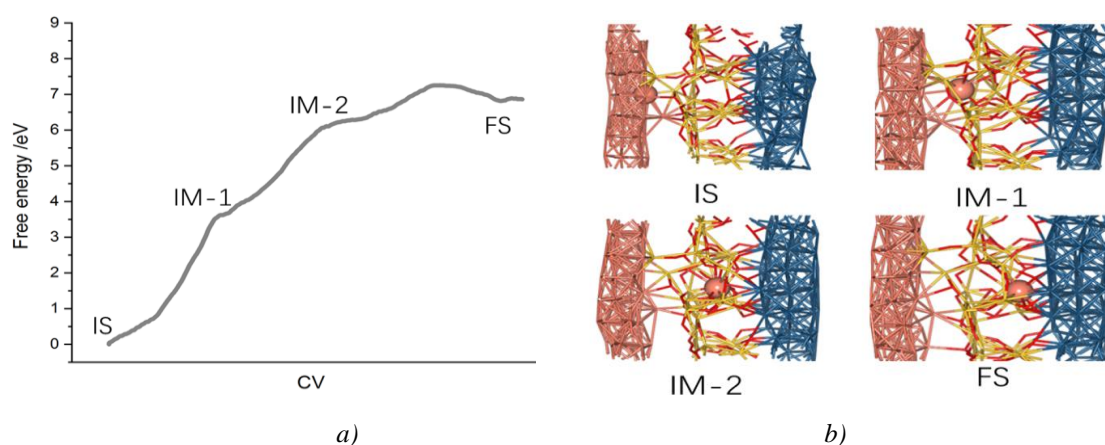


Fig. 3. (a) The energy change as a function of CV during the Cu diffusion from Cu (100)/SiO₂ (111) interface to the interface of SiO₂ (111)/Pt (100), and (b) the structure snapshots of different transitional states where the energy changes are calculated.

When considering the diffusion from the Cu (100)/SiO₂ (111) interface to the SiO₂ (111)/Pt (100), the calculated energy change results in Figure 3(a) with their corresponding state structures given in Figure 3(b). It is clear that the energy increases rapidly as the diffusing process proceeds. Since the SiO₂ (111) surface has stable quartz-like structure and the diffusion of the Cu ion would change the SiO₂(111) structure, the overall energy change of the Cu ion is ~ 7 eV to pass through the SiO₂

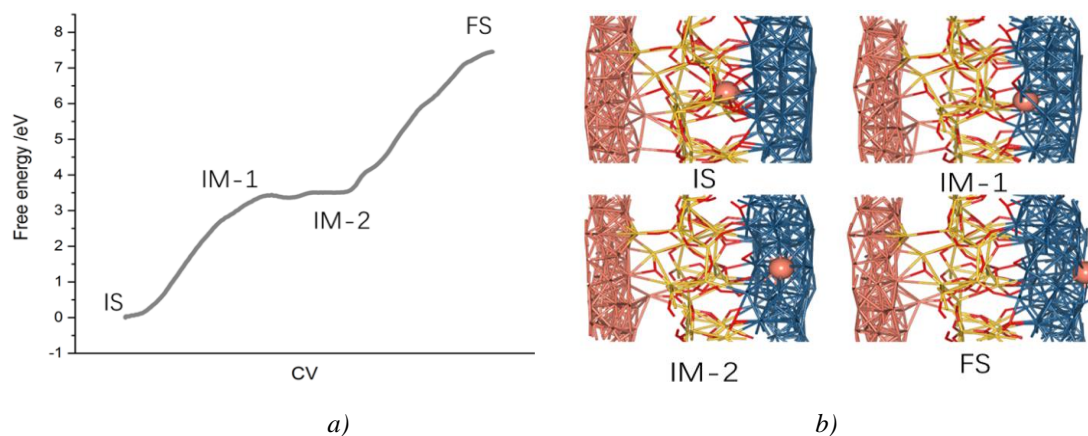


Fig. 4. (a) The energy change as a function of CV during the diffusion from SiO₂ (111)/Pt (100) interface to the interface between Pt (100) and vacuum. And (b) the structure snapshots of different transitional states where the energy changes are calculated.

Layer. It is also noted that the diffusion energy change is also related with the width of the studied stack. There are seven atomic layers for the SiO₂ (111) structure investigated here, and hence it is predicted that the average energy gain of the diffusion is 1 eV for each atom layer of SiO₂ (111). The Cu atom is continuously diffusing through the Pt layer, and the calculated energy change associated with the corresponding transitional atomic structures are illustrated in Figures 4(a) and 4(b), respectively. The overall energy change is ~ 7.5 eV, which is similar to that diffusing

through the SiO₂(111) layer. During this diffusing process, the insertion of the Cu ion into the Pt lattice is found difficult (from IS to IM-1 state) owing to the energy barrier of 3.25 eV. In fact, the Cu ion would be readily solvated into the Pt lattice since the considered Pt (100) surface is not a highly dense-compacted surface. Therefore, it is believed that the insertion of the Cu ion into the Pt (100) has the largest barrier during the diffusion from SiO₂ (111) to Pt (100). In Figure 4, the Cu ion does not fully contact with the Pt (100), and is still bonded with the O atoms from SiO₂. As a result, the role of the barrier of IS to IM-1 state may be overestimated. Considering that the diffusion from SiO₂ to Pt (100) involves two phases, the overall energy gain during the Cu ion diffusion from SiO₂ (111) to Pt (100) is predicted to be 1.63 eV.

In general, the diffusion of the Cu ion may overcome different energy barriers of 0.6 eV, 1 eV and 1.63 eV to diffuse through each layer of Cu (100), SiO₂ (111) and Pt (100) materials, respectively. Such barriers can be regarded as the capability of the Cu ion to diffuse through the corresponding materials, and the overall barrier of the Cu ion diffusing through the Cu/SiO₂/Pt structure should have the largest value within aforementioned energy barriers, i.e., the overall barrier is estimated to be 1.63 eV. According to the formula below, the calculated diffusion barrier can be implemented to compute the diffusion coefficient D:

$$D = \left(\frac{\delta^2 \times \nu \times q}{6 \times k_B \times T} \right) \times \exp \left(\frac{-E_a}{k_B \times T} \right) \quad (3)$$

where δ means the length of the diffusion; ν indicates the vibrational frequencies of the diffusing Cu ion; q represents the amount of electron charge, and we considered a fully charged Cu²⁺ and the calculated frequency is 1.85 THz. K_B means the Boltzmann constant, and T is temperature.

The obtained diffusion coefficients are shown in Figure 5. Although the diffusion coefficient is low under room temperatures, it increases rapidly with raising temperatures. At even higher temperatures, the diffusion coefficient would be even higher, meaning that the diffusion coefficient is strongly dependent on temperatures.

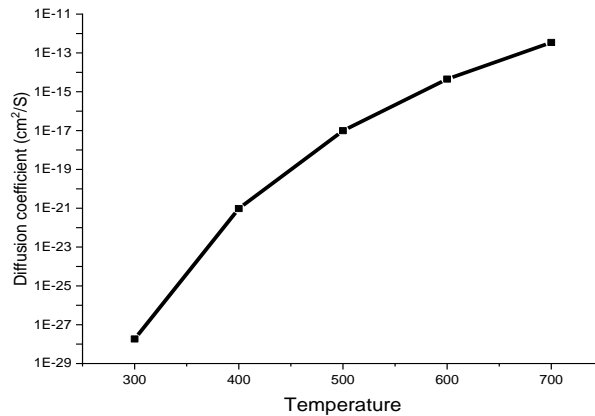


Fig. 5. Diffusion coefficient as a function of temperature during the diffusion of the Cu ion through the Cu/SiO₂/Pt heterojunction structure.

In addition, we further calculated the mobility plot as a function of the temperature (Figure 6) during the Cu ion diffusion process based on the formula:

$$\mu = D / (k_B T) \quad (4)$$

Following the trend in Figure 5, the calculated mobility of the Cu ion when diffusing through the studied heterojunction exhibit small values under low temperatures, and experiences a rapid increase along with temperature.

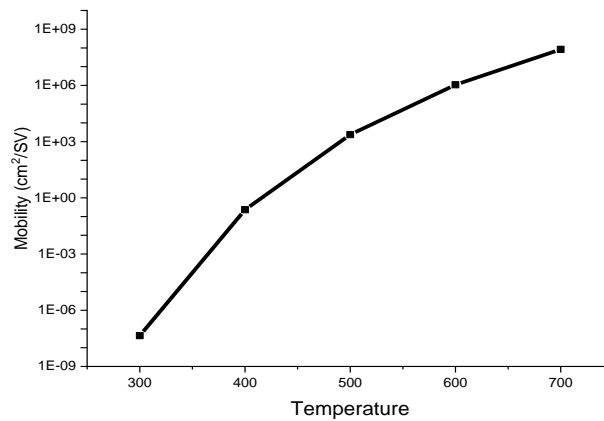


Fig. 6. Mobility as a function of temperature during the diffusion of the Cu ion through the Cu/SiO₂/Pt heterojunction material.

The ion electrical conductivity induced from the diffusion of the Cu ion is further obtained by the formula: $\sigma = \mu \cdot n \cdot q$, where n indicates the charge of the ion, giving rise to Figure 7. The ion electrical conductivity at room temperatures remains as low as 10^{-26} S/cm, meaning that the electrical conductivity contributed from the Cu ion diffusion is rather low. Such low ion electrical conductivity may arise from the high diffusion barrier from SiO₂ (111) phase to Pt (100) phase. The overall electrical conductivity comprises ionic conductivity and electron conductivity. Although the ionic conductivity is low in this case, the overall electrical conductivity of the Cu/SiO₂/Pt heterojunction in this case is dominated by the electronic structure and its electron conductivity. For this purpose, the density of states and the band structure so the Cu/SiO₂/Pt heterojunction is calculated, which can be used to determine the electron conductivity of the studied stack.

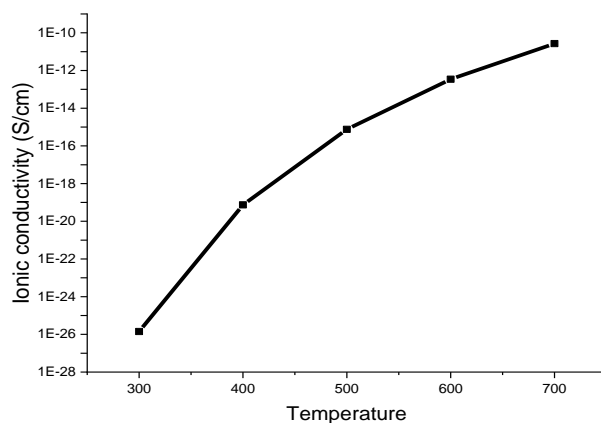


Fig. 7. Calculated ionic electrical conductivity as a function of temperature during the diffusion of the Cu ion through the Cu/SiO₂/Pt heterojunction.

We further studied the electronic structure of the Cu/SiO₂/Pt heterojunction structure. The calculated density of states is illustrated in Figure 8(a). It is clear that the overall

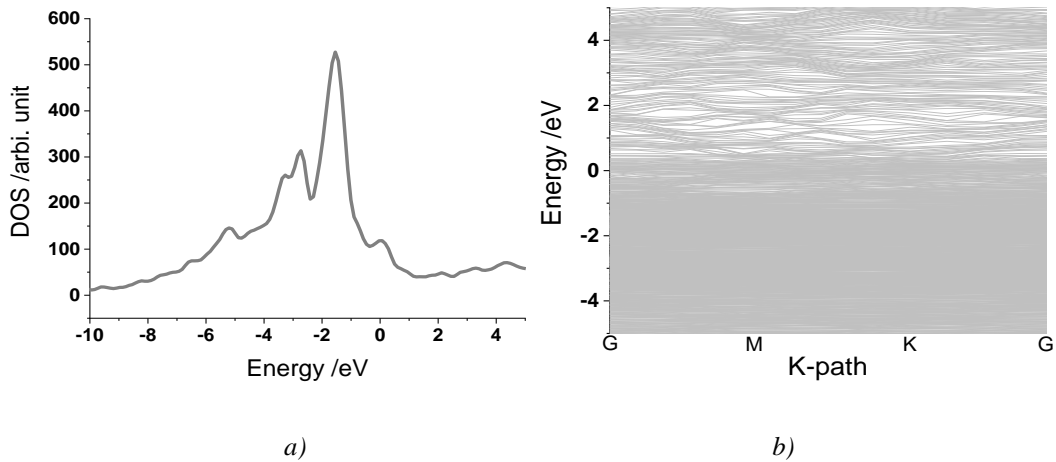


Fig. 8. (a) Density of states of the Cu/SiO₂/Pt structure. The energy of 0 corresponds to the Fermi level, and (b) band structure of the Cu/SiO₂/Pt structure. The energy of 0 corresponds to the Fermi level.

Structure has no bandgap around Fermi level, suggesting that the structure is electrically conductive. Although the SiO₂ lies in between the Pt and Cu layers, the electrons from the Pt and Cu metals can still transfer through the SiO₂ to enhance the electron transition of the pristine SiO₂. The main peak of the density of state is located at the -1.7 eV against the Fermi level, and this suggests that each part of the overall structure is highly interacted or bonded with other parts, also reflecting good stability of the structure. The band structure plot is shown in Figure 8(b). Similar to the results in Figure 8(a), the band structure shows no band-gaps, which again presents the good electrically conductive property of Cu/SiO₂/Pt structure. In addition, the bands are somewhat dense at the regions between -4 to 0 eV, consistent with the results in Figure 8(a) that the density of state values are relatively large at that region. Combined with the results of density of states and band calculations, the Cu/SiO₂/Pt structure is demonstrated to have high electron conductive property. Accordingly, although the ionic electrical conductivity of the Cu/SiO₂/Pt structure is small at room temperatures, the electron electrical conductivity of Cu/SiO₂/Pt is estimated to be fairly large. Considering the overall electrical conductivity equal to the sum of the ionic conductivity and the electric conductivity, it is possible that Cu/SiO₂/Pt may still maintain good electrical conduction, which in turn facilitates the diffusion of Cu ions through the heterojunction.

4. Conclusions

The electronic structure and electronic properties of one typical resistive memristor stack (Cu/SiO₂/Pt) is studied in details according to density functional theory and *ab initio* molecular dynamic simulations. Different energy barriers are found when the Cu ion crosses the entire Cu/SiO₂/Pt stack, and the overall energy barrier is calculated to be 1.63 eV. Further results also reveal that the diffusion coefficient and mobility of the Cu ions when diffusing through the stack fully depend on the temperature, and exhibit semiconductor characteristics. However, the ionic electrical conductivity remains relatively low, while the electron electrical conductivity follows the trend of the metal characteristic. The combination of these two parts therefore renders the heterojunction with great electrical conduction property, which makes it suitable for memristor applications.

References

- [1] T. N. Thesis, H. S. P. Wong, *Computing in Science & Engineering* 19, 41 (2017); <https://doi.org/10.1109/MCSE.2017.29>
- [2] S. Manipatruni, D. E. Nikonov, I. A. Young, *Nature Physics* 14, 338 (2018); <https://doi.org/10.1038/s41567-018-0101-4>
- [3] A. D. Franklin, *Science* 349(aab), 2750 (2015); <https://doi.org/10.1126/science.aab2750>
- [4] S. Kim, G. Myeong, W. Shin, H. Lim, B. Kim, T. Jin, S. Chang, K. Watanabe, T. Taniguchi, S. Cho, *Nature Nanotechnology* 15, 203 (2020); <https://doi.org/10.1038/s41565-019-0623-7>
- [5] M. M. Vopson, X. L. Tan, *IEEE Electron Device Letters* 37, 1551 (2016); <https://doi.org/10.1109/LED.2016.2614841>
- [6] M. I. Rashid, F. Ferdous, B. M. S. B. Talukder, P. Henny, A. N. Beal, M. T. Rahman, *IEEE Transactions on Very Large Scale Integration (VLSI) Systems* 29, 14 (2021); <https://doi.org/10.1109/TVLSI.2020.3018998>
- [7] S. Ikegawa, F. B. Mancoff, J. Janesky, S. Aggarwal, *IEEE Transactions on Electron Devices* 67, 1407 (2020); <https://doi.org/10.1109/TED.2020.2965403>
- [8] H. Lee, A. Lee, F. Ebrahimi, P. K. Amiri, K. L. Wang, *IEEE Magnetics Letters* 8,4305905 (2017); <https://doi.org/10.1109/LMAG.2017.2693963>
- [9] L. Wang, L. Tu, J. Wen, *Science and Technology of Advanced Materials* 18, 406 (2017); <https://doi.org/10.1080/14686996.2017.1332455>
- [10] Y. Kwon, B. Park, D. H. Kang, *IEEE Electron Device Letters* 36, 454 (2015); <https://doi.org/10.1109/LED.2015.2414952>
- [11] F. Zahoor, T. Z. A. Zulkifli, F. A. Khanday, *Nanoscale Research Letters* 15, 90 (2020); <https://doi.org/10.1186/s11671-020-03299-9>
- [12] Y. H. Zhang, Z. W. Wang, T. Shi, C. Bi, F. Rao, Y. M. Cai, Q. Liu, H. Q. Wu, P. Zhou, *INFOMAT* 2, 261 (2020); <https://doi.org/10.1002/inf2.12077>
- [13] K. G. Young-Eisher, G. Bersuker, B. Butcher, A. Padovani, L. Larcher, D. Veksler, D. C. Gilmer, *IEEE Electron Device Letters* 34, 750 (2013); <https://doi.org/10.1109/LED.2013.2256101>
- [14] S. Deswal, A. Kumar, A. Kumar, *AIP Advances* 8, 085014 (2018); <https://doi.org/10.1063/1.5040466>
- [15] V. A. Voronkovskii, V. S. Aliev, A. K. Gerasimova, D. R. Islamov, *Materials Research Express* 5, 016402 (2018); <https://doi.org/10.1088/2053-1591/aaa099>
- [16] Z. W. Zheng, H. H. Hsu, C. H. Cheng, P. C. Chen, *Physica Status Solidi-Rapid Research Letter* 8, 431 (2014); <https://doi.org/10.1002/pssr.201409039>
- [17] L. O. Chua, *IEEE Transactions on Circuit Theory CT* 18, 507 (1971); <https://doi.org/10.1109/TCT.1971.1083337>
- [18] D. B. Strukov, G. S. Snider, D. R. Stewart, R. S. Williams, *Nature* 453, 80 (2008); <https://doi.org/10.1038/nature06932>
- [19] H. S. Alagoz, M. Davies, Y. Zhong, K. H. Chow, J. Jung, *Solid State Communications* 303, 113718 (2019); <https://doi.org/10.1016/j.ssc.2019.113718>
- [20] G. Gul, *Applied Nanoscience* 10, 611 (2019); <https://doi.org/10.1007/s13204-019-01179-y>
- [21] L. Tang, H. Maruyama, T. H. Han, J. C. Nino, Y. H. Chen, D. Zhang, *Applied Surf Sci.* 515,

- 146015 (2020); <https://doi.org/10.1016/j.apsusc.2020.146015>
- [22] V. Mikheev, A. Chouprik, Y. Lebedinskii, S. Zarubin, A. M. Markeev, A. V. Zenkevich, D. Negrov, *Nanotechnology* 31, 215205 (2020); <https://doi.org/10.1088/1361-6528/ab746d>
- [23] X. B. Yan, C. Y. Qin, C. Lu, J. H. Zhao, R. J. Zhao, D. L. Ren, Z. Y. Zhou, H. Wang, J. J. Wang, L. Zhang, X. Y. Li, Y. F. Pei, G. Wang, Q. L. Zhao, K. Y. Wang, Z. A. Xiao, H. Li, *ACS Applied Materials Interfaces* 11, 48029 (2019); <https://doi.org/10.1021/acsami.9b17160>
- [24] S. Lee, W. R. Zhang, F. Khatkhatay, H. Y. Wang, Q. X. Jia, J. L. MacManus-Driscoll, *Nano Letters* 15, 7362 (2015); <https://doi.org/10.1021/acs.nanolett.5b02726>
- [25] J. F. Sevic, N. P. Kobayashi, *Applied Physics Letters* 111, 153107 (2017); <https://doi.org/10.1063/1.5003168>
- [26] J. Y. Chen, C. W. Huang, C. H. Chiu, Y. T. Huang, W. W. Wu, *Advanced Materials* 27, 5028 (2015); <https://doi.org/10.1002/adma.201502758>
- [27] Q. Gao, A. P. Huang, Q. Hu, X. J. Zhang, Y. Chi, R. M. Li, Y. H. Ji, X. L. Chen, R. M. Zhao, M. Wang, H. L. Shi, M. Wang, Y. M. Cui, Z. Xiao, P. K. Chu, *ACS Applied Materials Interface* 11, 21734 (2019); <https://doi.org/10.1021/acsami.9b06855>
- [28] V. A. Volodin, G. N. Kamaev, V. A. Gritsenko, A. A. Gismatulin, A. Chin, M. Vergnat, *Applied Physics Letters* 114, 233104 (2019); <https://doi.org/10.1063/1.5079690>
- [29] L. Wang, C. H. Yang, J. Wen, S. Gai, Y. X. Peng, *Journal of Materials Science-Materials in Electronics* 26, 4618 (2015); <https://doi.org/10.1007/s10854-015-2848-z>
- [30] G. Kresse, J. Furthmuller, *Physical Review B* 54, 11169 (1996); <https://doi.org/10.1103/PhysRevB.54.11169>
- [31] J. Hafner, *Journal of Computational Chemistry* 29, 2044 (2008); <https://doi.org/10.1002/jcc.21057>
- [32] D. Hobbs, G. Kresse, J. Hafner, *Physical Review B* 62, 11556 (2000); <https://doi.org/10.1103/PhysRevB.62.11556>